A study of electric dipole radiation via scattering of polarized laser light

Natthi L. Sharma,[a)] Ernest R. Behringer, and Rene C. Crombez
Department of Physics and Astronomy, Eastern Michigan University, Ypsilanti, Michigan 48197

We have developed an advanced undergraduate experiment to explore electric dipole radiation in the optical frequency domain. A polarized laser beam is used to illuminate an aqueous suspension of skim milk, and the light scattered from the suspension is measured in the plane perpendicular to the laser beam as a function of the angle θ with respect to the polarization direction and as a function of the perpendicular distance R from the laser beam. When the length of the scattering region, d, is much smaller than R, the measurements agree very well with the $\sin^2\theta/R^2$ dependence of electric dipole radiation. Increasing the scatterer concentration increases the background of multiply scattered light and decreases the degree of polarization of the scattered light with no appreciable change in the observed $\sin^2\theta/R^2$ dependence. We discuss variations of the experiment for different instructional needs and describe how an understanding of dipole radiation helps students to appreciate a number of optical phenomena. © *2003 American Association of Physics Teachers.*
[DOI: 10.1119/1.1575764]

I. INTRODUCTION

Because of its abstract nature relative to mechanics, electromagnetism is usually considered to be more difficult to learn. Consequently, it is desirable to develop demonstrations and laboratory experiments that vividly and effectively illustrate various phenomena in electromagnetism. One such phenomenon is that an accelerated charge does not radiate in the direction of its acceleration. A related phenomenon is that the light scattered at 90° from an unpolarized beam becomes polarized. Still another one is that a charge rotating in a circle radiates circularly polarized electromagnetic (EM) waves as observed from a point on the axis of the circle, but a linearly polarized wave when observed from a point in the plane of the circle. Understanding the physics underlying electric dipole radiation helps us to understand such phenomena. Moreover, electric dipole radiation is the model for the strongest interaction between matter and light. For these reasons, it would be beneficial to have students perform a laboratory experiment in which they can investigate dipole radiation.

The inspiration for the work described here came while one of us (NLS) was visiting a femtosecond laser pulse facility and noticed an interesting phenomenon. The path of the beam from a 5-W vertically polarized continuous wave argon laser that was quite visible from the side became *invisible* when observed from above the beam. This effect was very intriguing for a few minutes; then it suddenly occurred to the observer that the effect could be explained by the scattering of light from the laser beam by air molecules acting as dipole radiators. The graduate students using the laser were so focused on their projects that they had neither noticed this phenomenon nor could explain it. Although this effect is easily observed with a few watt argon laser in a relatively dust-free room, we have subsequently found that a 50-mW polarized He–Ne laser is sufficient for a visual demonstration. With low power (<20-mW) lasers, this effect is barely observable in air. To enhance this effect (especially with commonly available, few milliwatt lasers), it is helpful to use a medium that has a greater density of scatterers than air. A readily available medium is an aqueous suspension of milk, and we have found that using a 5- to 10-mW polarized helium–neon laser or even a diode laser (for example, a hand-held laser pointer) is sufficient for a visual display in a lecture demonstration.

We have developed an undergraduate laboratory experiment for quantitative exploration of electric dipole radiation in the optical frequency domain. In particular, a polarized laser beam is used to illuminate aqueous suspensions of skim milk. The resulting scattered light is analyzed for its angular and radial dependence in the plane perpendicular to the laser beam. The experiment elucidates the main features of electric dipole radiation in a way that is easily observed and could be used to augment the study of dipole radiation in the advanced undergraduate course in electromagnetism. The combination of rich physics and its easy observation led us to choose this experiment as the first of six experiments that we developed for a new undergraduate laboratory course in modern optics.[1] This experiment helped the students to understand and appreciate many related phenomena that occur in subsequent experiments of the course.

Several light scattering experiments suitable for an advanced undergraduate laboratory have been previously described in the literature. Shaw, Hones, and Wunderlich studied the polarization of light scattered from an unpolarized beam, but not the scattering of polarized light.[2] There also have been studies of scattering of polarized and unpolarized light from particulate suspensions with particle size greater than the light wavelength based on an approximate form of Mie theory.[3–6] The wavelength dependence of light scattering has also been studied, both in the Rayleigh and Mie regimes.[7,8] Bohren studied the effects of multiple scattering, which become significant only when the concentration and/or optical thickness of scatterers becomes large, with the help of a two-stream theory.[9] The only study that we have found that deals with the angular distribution of scattered polarized light is by George *et al.*, who studied the scattering of polarized light from gas atoms.[10] This work, however, contains a large discrepancy between theory and experiment which the authors did not explain.

In the following, we discuss the associated theory, describe the experiment, present the data, and discuss the results. We then discuss how the understanding of dipole ra-

diation developed in this experiment can be applied to help students build an understanding of related phenomena.

II. THEORY

We begin this section by briefly reviewing light scattering. We then introduce the radiation fields produced by an electric dipole or an accelerated charge and describe the scattered light as the radiation from induced electric dipoles driven by the incident light.

Light scattering is so ubiquitous that virtually every aspect of wave optics is an example of scattering.[11] In general, scattering involves energy–momentum exchange between two systems while the two systems interact. The special case of scattering in which there is no energy exchange is called elastic. Otherwise, the scattering is inelastic. Elastic scattering is useful for studying the size and spatial arrangement of system constituents, as is the case of diffraction of light from slits or x-ray diffraction from crystals. Inelastic scattering often is used to study the internal dynamics (for example, energy levels in an atom) of one of the systems if that of the other is simple and known, as is the case for photoluminescence and Raman scattering.

An atom not only scatters light but creates its own light at various characteristic frequencies. If the frequency of incident light does not match any of these characteristic frequencies, then the electrons of the target atoms are driven into forced oscillations about the positively charged nucleus by the electric field of the incident EM wave, that is, the electrons oscillate in the direction of polarization of the incident wave with a frequency equal to that of the incident light. These oscillating charges produce their own (electric dipole) radiation, which is elastically scattered incident light. As the frequency of incident light approaches one of the resonance frequencies of the atoms, the amplitude of oscillations of the charges and the probability of scattering becomes large.

The intensity distribution of light that is scattered depends on the intensity, frequency, and state of polarization of the incident radiation and on the concentration, spatial arrangement, size, and optical properties of the scatterers. The exact form of the angular distribution of the scattered light is governed by the superposition of the fields generated by the electric and magnetic multipoles induced in the scatterers by the incident light, and will in general depend on the state of polarization of the incident light. In dense uniform materials such as transparent liquids and solids, that is, materials with atomic separations much less than the wavelength λ of the incident light, the scattering of light is very weak. This is because the number of oscillators in a cube of linear dimension λ is very large, and the wavelets that these oscillators emit tend to interfere destructively in all except the forward direction.[12] The phenomenon of forward scattering is an example of coherent scattering, which occurs when the oscillator spacing is much smaller than the wavelength of incident light. Reflection and refraction at oblique incidence are also special cases of coherent scattering.[11] An example of a uniform, dense medium in which there is hardly any scattering is pure water. However, the presence of density fluctuations or of randomly located and sparsely dispersed (separation much greater than λ) impurities in transparent liquids and solids enhances light scattering. In this case, the lack of phase correlation among wavelets scattered from randomly distributed impurities results in incoherent scattering, in which the total intensity is the sum of the individual wavelet

intensities. For atomic or molecular scatterers with characteristic size s smaller than about $\lambda/20$, the dominant part of the scattered radiation at large distances ($r \gg \lambda$) is the contribution due to the electric dipole part of the charge oscillations with a typical $1/\lambda^4$ wavelength dependence and is called Rayleigh scattering. This wavelength dependence leads to preferential scattering of blue light and is responsible for both the blue sky and the reddish-yellow sunrise/sunset. It is for the same reason that a glass of water mixed with a few drops of milk acquires a blue tinge when observed at angles greater than 90° from the direction of a flashlight beam passing through the milk suspension. The remaining transmitted light then appears to have a yellow-red tinge.

If the size of the scatterers is comparable to or larger than the wavelength ($s \approx \lambda$), the contributions due to quadrupole and higher order multipoles induced by the incident field have to be taken into account. These multipole contributions change the wavelength dependence and angular distribution of the scattered light.[13,14] As s increases, the wavelength dependence weakens. When $s \approx 20\lambda$, there is hardly any wavelength dependence left, and the scattering is known as Mie scattering.[15] Scattering from clouds, fog, or skim milk are examples of Mie scattering. The weak wavelength dependence of Mie scattering can be demonstrated with a glass of hot water fresh from a faucet in which tiny air bubbles are present: it appears whitish until the bubbles escape. As the size of the scatterers increases further, the particles begin to scatter preferentially in the forward direction. If the concentration of these large scatterers is high, there will be multiple scattering (that is, scattering of scattered light) as well. In the case where the scatterers are transparent, multiple scattering is responsible for the bright whiteness of snow, salt, and powdered glass (even from colored bottles), all of which are comprised of a dense collection of millimeter size transparent grains suspended in a transparent medium.[9]

In the rest of this paper, we assume that the size of the scatterers is small compared to the wavelength of the incident light, that is, $s \ll \lambda$. Consequently, we limit ourselves to the study of the electric dipole contribution to the scattered light.

Electric dipole radiation. An oscillating, localized charge distribution of size $s \ll \lambda$ produces fields in the radiation zone ($r \gg \lambda$) that are given by the electric–dipole radiation fields[16]

$$\mathbf{E}(\mathbf{r},t) = \frac{\mu_0}{4\pi r} \hat{\mathbf{r}} \times \left[\hat{\mathbf{r}} \times \left(\frac{d^2 \mathbf{p}}{dt^2} \right)_{t-(r/c)} \right], \tag{1}$$

and

$$\mathbf{B}(\mathbf{r},t) = \frac{1}{c} \hat{\mathbf{r}} \times E(\mathbf{r},t), \tag{2}$$

where $\mathbf{p}$ is the induced dipole moment of the charge distribution and $t-(r/c) \equiv t_{\text{ret}}$ is the retarded time.

For a single point charge q, the dipole moment is given by $\mathbf{p}=q\mathbf{s}$, where $\mathbf{s}$ is the position vector of q at time t. Equation (1) may then be written as

$$\mathbf{E}(\mathbf{r},t) = \frac{\mu_0 q}{4\pi} \frac{[\hat{\mathbf{r}} \times [\hat{\mathbf{r}} \times \mathbf{a}(t_{\text{ret}})]]}{r}, \tag{3}$$

where $\mathbf{a}=\ddot{\mathbf{s}}=(1/q)d^2\mathbf{p}/dt^2$ is the acceleration of the point charge q. We denote the component of the acceleration $\mathbf{a}$ that is perpendicular to the field position vector $\mathbf{r}$ by $\mathbf{a}_\perp$. The
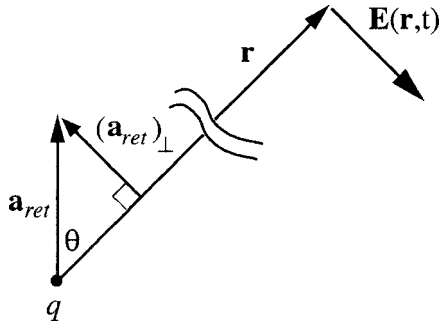
Fig. 1. The relation between $\mathbf{a}_{\text{ret}} = \mathbf{a}(t_{\text{ret}})$, $(\mathbf{a}_{\text{ret}})_\perp$, $\mathbf{r}$, and $\mathbf{E}(\mathbf{r},t)$ for an accelerated charge q. Note that the acceleration vector at the retarded time $t - r/c$ give rise to the electric field vector at time t; also, $\mathbf{E}(\mathbf{r},t)$ is opposite to $(\mathbf{a}_{\text{ret}})_\perp$.
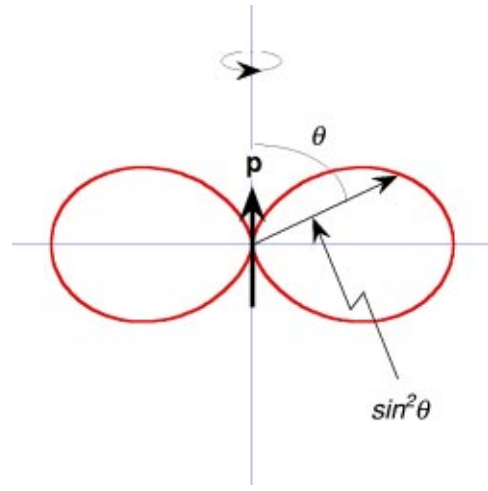

Fig. 2. Polar plot of the angular distribution of electric dipole radiation. For an accelerated charge $\mathbf{p}$ is replaced by $\mathbf{a}$. The symmetry axis is the dipole axis or the direction of acceleration for an accelerated charge.

relationships between $\mathbf{a}$, $\mathbf{r}$, and $\mathbf{a}_\perp$ are shown in Fig. 1. It follows that $\hat{\mathbf{r}} \times [\hat{\mathbf{r}} \times \mathbf{a}] = -\mathbf{a}_\perp$, and the substitution of this relation into Eq. (3) yields[17,18]

$$\mathbf{E}(\mathbf{r},t) = -\frac{q}{4\pi\epsilon_0 c^2} \frac{\mathbf{a}_\perp(t_{\text{ret}})}{r}. \tag{4}$$

The corresponding $\mathbf{B}$ field is obtained by inserting Eq. (4) into Eq. (2).

If the direction of observation $\hat{\mathbf{r}}$ makes an angle θ with the direction of acceleration $\mathbf{a}$ as shown in Fig. 1, then $a_\perp = a \sin\theta$ and the magnitude of $\mathbf{E}$ becomes

$$E(r,\theta;t) = \frac{q}{4\pi\epsilon_0 c^2} \frac{a_{\text{ret}}\sin\theta}{r}, \tag{5}$$

where $a_{\text{ret}} = a(t_{\text{ret}})$.

Now suppose that the charge q is an electron in an atom, driven into oscillations about the positively charged nucleus by the electric field $\hat{\mathbf{z}}E_0 \cos\omega t$ of an incident light wave. If we neglect damping, the equation of motion of the charge q is

$$m\ddot{z} = qE_0 \cos\omega t - m\omega_0^2 z, \tag{6}$$

where m is the mass and ω_0 is the smallest atomic resonance frequency of q. A solution to this undamped driven harmonic oscillator is given by

$$z = \frac{qE_0 \cos\omega t}{m(\omega_0^2 - \omega^2)}, \tag{7}$$

as can be verified by substitution. Consequently, the acceleration of charge q at t_{ret} is

$$a_{\text{ret}} = \ddot{z}(t_{\text{ret}}) = -\omega^2 \frac{qE_0 \cos\omega t_{\text{ret}}}{m(\omega_0^2 - \omega^2)}. \tag{8}$$

For most transparent materials, the resonance frequency $\omega_0 \gg \omega$, if ω corresponds to the visible region. Therefore, if we neglect ω in comparison to ω_0 in the denominator of Eq. (8), we obtain

$$a_{\text{ret}} = -\frac{q}{m} \frac{\omega^2}{\omega_0^2} E_0 \cos\omega t_{\text{ret}}. \tag{9}$$

If we substitute a_{ret} from Eq. (9) into Eq. (5), we obtain

$$E(r,\theta;t) = -\frac{\omega^2}{\omega_0^2} \frac{r_0}{r} \sin\theta E_0 \cos\omega t_{\text{ret}}, \tag{10}$$

where $r_0 = q^2/(4\pi\epsilon_0 mc^2)$ is the classical electron radius if q is the electron charge.

In a neutral atom with atomic number Z, there are Z electrons. If the wavelength λ of the incident light is much larger than the atomic size (dipole approximation), all the Z electrons are driven in phase and the resulting electric field due to an atom of atomic number Z is

$$E(r,\theta;t) = -Z\frac{\omega^2}{\omega_0^2} \frac{r_0}{r} \sin\theta E_0 \cos\omega t_{\text{ret}}. \tag{11}$$

The intensity distribution of the light scattered by an atomic dipole is then

$$I(\omega,r,\theta) = \epsilon_0 c \langle E^2 \rangle = I_{\text{inc}} Z^2 \frac{\omega^4}{\omega_0^4} \frac{r_0^2}{r^2} \sin^2\theta, \tag{12}$$

where $I_{\text{inc}} = \frac{1}{2}\epsilon_0 c E_0^2$ is the intensity of the incident wave; the factor of 1/2 arises from the time averaging of $\cos^2\omega t_{\text{ret}}$. Equation (12) contains the ω^4 frequency dependence predicted by Rayleigh.[19] Note that the angle θ is measured from the dipole axis, which in our case is the same as the direction of polarization of the incident light, that is, along the z axis. The scattered intensity increases as $\sin^2\theta$. A polar plot of this angular distribution is shown in Fig. 2. Because of cylindrical symmetry, the radiation is independent of the azimuthal angle and the angular distribution in three dimensions acquires a doughnut shape that is obtained by rotating Fig. 2 about the dipole axis. The oscillating dipole radiates most efficiently around its "waist," or equator ($\theta = \pi/2$); there is no radiation along its axis ($\theta = 0$). The intensity of radiation varies as $1/r^2$ from the location of the dipole.

Equation (12) describes the intensity distribution in the radiation zone ($r \gg \lambda$) which results from a single point dipole or a finite size dipole source (of size d) that satisfies $d \ll \lambda \ll r$, as for an atomic or molecular dipole emitting visible radiation. In the experiment described in Sec. III, many scatterers are illuminated by a polarized laser beam and
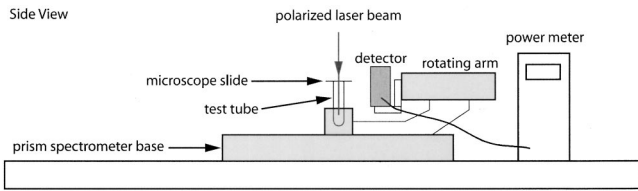
Fig. 3. The polarized laser beam travels downward and impinges on the microscope slide covering the test tube. An old prism spectrometer table holds the test tube in place and enables the rotation of the optical detector in the plane perpendicular to the beam.
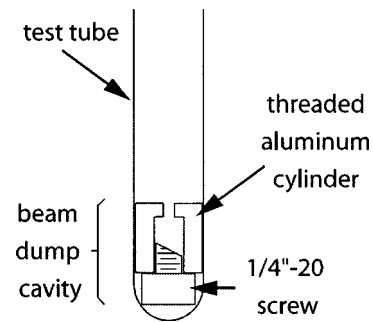

Fig. 4. Schematic diagram of the beam dump cavity. The cavity is made from a cylindrical piece of aluminum and tapped for a 1/4-in.-20 screw on one end and with a through hole just larger than the laser beam on the other end. A screw that is ground at an angle serves to diffusely reflect the beam into the cavity and reduces the background light in the experiment.

thereby contribute to the intensity of scattered light. To simplify the analysis, we make two assumptions here. First, the detector area and the size of the scattering region are small enough (compared to r) so that the variation in r and θ from the detector to various dipole scatterers can be neglected, thus enabling us to use a common value of $\sin \theta / r$ for all the dipoles, evaluated from the center of the scattering region to the center of the detector. Second, the spatial distribution of the scatterers in the suspension is assumed to be random. The random distribution of scatterers implies incoherent scattering (no interference effects), and the total scattered light intensity is simply obtained by multiplying the scattered intensity due to a single dipole by the total number, N, of dipoles involved. We then obtain from Eq. (12) the total scattered intensity

$$I(R, \theta) = NZ^2 I_{\text{inc}} \frac{\omega^4}{\omega_0^4} \frac{r_0^2}{R^2} \sin^2 \theta, \qquad (13)$$

where we have replaced r by R in the plane perpendicular to the beam, as in the experiments described in Sec III. A small detector with effective area $d\mathbf{A}$ and located at (R, θ) will then register an average power given by $dP(R, \theta) = I(R, \theta) d\mathbf{A} \cdot \hat{\mathbf{R}}$, where $\hat{\mathbf{R}}$ is the unit vector pointing from the center of the scattering region to the center of the detector.

III. EXPERIMENT

We used a horizontally polarized laser beam (with its $\mathbf{E}$ field along the z axis) traveling vertically down along the (x) axis of a test tube to illuminate an aqueous suspension of skim milk and measured the angular and radial distributions of light scattered into the plane perpendicular (yz plane) to the beam. We also measured the degree of polarization of the scattered light as a function of concentration. Because we used a fixed frequency laser as the light source, we did not study the frequency dependence of the scattered light intensity. In the following, we describe the equipment and procedures used to make the measurements.

To measure the angular distributions, we used an old prism spectrometer with the following modifications (see Fig. 3). First, we replaced the prism table with a glass test tube mounted in a cylindrical aluminum sleeve specially machined to snugly fit with the prism table holder. This modification allowed us to align the axis of the test tube with the axis of the spectrometer. Second, we removed the telescope in the rotating arm and replaced it with an assembly for an optical detector. This assembly consisted of a steel cylinder that snugly fit into the rotating arm, and two aluminum pieces to support the Newport Model 818-SL detector that was used with a Newport Model 840-C Optical Power

Meter.[20] An aperture, approximately 4 mm in diameter, was attached to the detector to reduce the amount of stray light entering the detector. The polarized beam was obtained from a polarized He–Ne laser.[21] The beam was directed vertically downward toward the test tube by either mounting the cylindrical laser head vertically or by using a polarizing beam splitter cube to deflect a horizontal beam into the vertically downward direction. The beam was made to travel along the axis of the tube containing the aqueous suspension by adjusting the two tilt screws in the laser mount. A homemade beam dump cavity consisting of a cylindrical aluminum tube and a 1/4-in.-20 screw was placed on the bottom of the test tube to eliminate retroreflection from the bottom of the tube. As shown in Fig. 4, the end of the screw is ground at an angle to diffusely scatter the beam into the cavity.

The test tube was filled to the brim and then covered with a microscope cover slip to prevent focusing of the beam by the liquid meniscus and to decrease the rate of evaporation. A piece of black paper that extended beyond the cover slip on the test tube was wrapped around the output end of the laser to prevent light scattered from the edges of the cover slip from reaching the detector. Finally, most of the test tube was covered with black electrical tape except for a portion centered on the axis of the detector. The length of the exposed scattering region was typically 3 mm, but was later varied from 0.6 mm to 5 cm to observe the effect on the angular and radial distribution of the scattered light. To measure the angular distribution of the scattered light, the arm carrying the detector was rotated in a horizontal circular path around the tube. The measurements were made at 5° intervals over a range of about 250° while rotating the arm in one direction. The measurements were immediately repeated in reverse order while rotating the arm in the opposite direction. In this way, the scattered power at each angular position was recorded twice, and these two values were averaged to compensate for any settling of the suspension, especially if it was freshly prepared. The measurements were performed in a completely dark room with the backlit power meter held under the table.

We measured the radial distributions using two sets of apparatus. The first set of apparatus consisted of the prism spectrometer and laser described above and an optical rail with a component carrier. The Newport detector was removed from the rotating arm of the spectrometer and mounted on the component carrier, thereby enabling the controlled radial positioning of the detector. The detector aper-

ture opening was carefully aligned with the exposed beam or the slit opening in the test tube using a second laser. The scattered power measurements were made at regular intervals over a range of about 10 cm. The power at each radial position was recorded twice: first, while translating the detector away from the test tube, and again while translating the detector back toward the test tube. As before, the two measurements were averaged to compensate for any settling of the suspension while the data were collected over several minutes. The two readings were found to agree within 1% if the suspension was dilute (about 1%) and already settled. Although the Newport Power Meter can be used to measure optical power as small as 0.1 nW, we could cover only a radial interval of about 10 cm before this limit was reached. Consequently, we used a second set of apparatus in which the spectrometer was removed and the suspension carrying test tube was mounted in a post holder on an optical rail. The Newport detector and power meter were, respectively, replaced with a photomultiplier tube and a hand-held digital multimeter.[22] The photomultiplier tube housing was attached to a component carrier using a homemade coupling. Because of the higher sensitivity of the photomultiplier tube, we were able to measure scattered light intensities over a radial interval of about 50 cm. One or more variable apertures were used to limit the size of the scattering region and the angular acceptance of the photomultiplier tube. We used Kaleidagraph[23] to plot and to generate fits to the data.

The degree of linear polarization of the scattered light as a function of concentration was measured using the same apparatus as for measuring the angular distributions. The degree of polarization is defined as $(I_{max}-I_{min})/(I_{max}+I_{min})$. The corresponding scattered powers were measured in the direction of maximum scattered light ($\theta=\pi/2$) by mounting a polarizer in front of the Newport detector and rotating the polarizer to obtain the maximum and minimum power meter readings. The detector-to-beam distance was kept at 8.0 cm and only a 3-mm-wide portion of the test tube was uncovered. The concentration was varied from 0.25 to 10% by volume.

The suspensions were prepared by mixing skim milk with distilled water. Skim milk contains mostly water and solids such as lactose and protein, and smaller amounts of minerals, acids, enzymes, gases, and vitamins.[24] Lactose, a disaccharide, is composed of the monosaccharides glucose and galactose, each of which has a carbon ring structure. The linear dimension of lactose is slightly less than 1 nm. Most of the protein in milk is in the form of caseins, long chain molecules that form micelles with diameters in the range of 10–300 nm, with a mean diameter of 15 nm.[25] The mean diameter of 15 nm is well below $\lambda/20$ for the He–Ne wavelength of 633 nm and hence meets the criteria of Rayleigh scattering.

IV. RESULTS AND DISCUSSION

The initial angular measurements were performed without a slit/aperture in front of the test tube, and $d\approx 5$-cm-long region of milk suspension (1% by volume) was exposed to the detector, located a distance of 6 cm from the beam center. As shown in the plot labeled (1%, 5 cm) in Fig. 5, the normalized power data fit well to $A+B\sin^2(\theta-\theta_0)$ with a nonzero constant offset A. This offset, which is the minimum scattered light, is about 18% of the maximum scattered signal. Its nonzero value implies that some light is radiated in
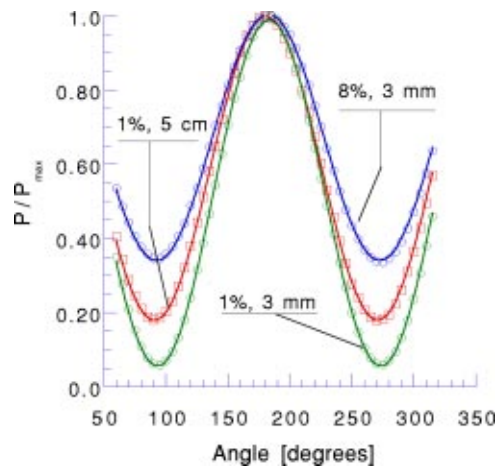

Fig. 5. Plot of normalized power vs angle for three experimental situations. The open symbols represent measurements and the solid curves represent fits of the function $A+B\sin^2(\theta-\theta_0)$ to the data. These data show the variation of the offset A due to either increasing the test tube slit size or to increasing the concentration of the aqueous suspension of skim milk. The concentrations by volume and the slit sizes are indicated.

the direction of the dipole axis $\theta=\theta_0$. To understand the origin of this offset, we first checked the purity of polarization of our laser and found it to be better than 400:1.[21] When we repeated the measurements on 1% milk with $d=3$ mm (by wrapping black tape around the test tube except for a 3-mm region centered on the axis of the detector), the offset value decreased to about 6% of the maximum signal as shown in the curve labeled (1%, 3 mm) in Fig. 5. After repeating the measurements with $d=3$ mm but increasing the milk concentration to 8%, the offset value jumped to 34%. This result is shown in the curve labeled (8%, 3 mm) in Fig. 5. Because decreasing the exposed tube length or the concentration reduces this background, we conclude that a large part (though not all) of the constant offset arises from multiple-scattered background light, that is, mostly the light from scatterers outside the region illuminated by the beam. From Eq. (4) we see that the **E** field of the induced dipoles is horizontal, that is, in the plane containing the dipole and the detector and perpendicular to the detector axis. Therefore a sheet polarizer, with its transmission axis horizontal and mounted in front of the detector, further reduced the background by allowing only the horizontally polarized light to pass. This result is shown separately in the lower curve in Fig. 6 for $d=3$ mm and a 1% milk suspension. The upper curve shows the measured power without the polarizer with an offset value of 6%. The offset with the polarizer (the lower curve) is reduced to merely 2.3% (or 3% after dividing by the transmission efficiency 0.76 of the HN-38 sheet polarizer). These curves are not normalized for the sake of clarity.

The value of the fitting parameter $\theta_0=93.3°$ in Fig. 6 corresponds to the orientation of the dipole axes of the induced dipoles, which is the same as the direction of polarization of the laser beam as was verified by checking the beam polarization before it enters the suspension. As we increased the concentration of scatterers from 0.25% to 10% for $d/R=0.05$, only the value of the constant offset A increased with no change in the $\sin^2\theta$ angular distribution. Evidence for this is shown in the fits for the 8% and 1% suspensions in Fig. 5.
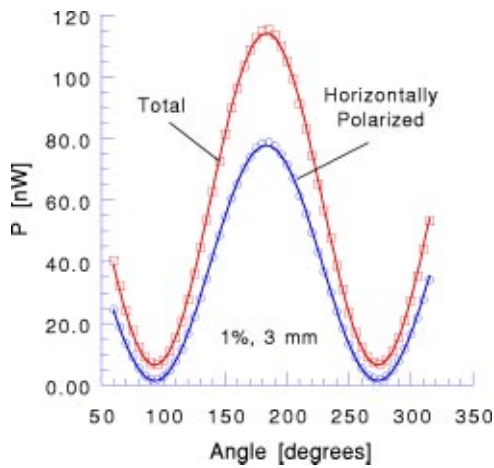
Fig. 6. Plot of power vs angle for a 1% by volume aqueous suspension of skim milk, measured with ("horizontally polarized") and without ("total") a sheet polarizer in front of the detector. The open symbols represent measurements and the solid curves represent fits of the function $A + B \sin^2(\theta - \theta_0)$ to the data.

Fig. 8. Plot of photomultiplier tube signal vs distance for different slit and aperture arrangements, as described in the text. The signal was measured at $\theta = 90°$, the direction in which the intensity of the scattered light is a maximum. The symbols represent measurements and the solid curves represent fits of the function $a/(r+b)^2$ to the data.

Next, we consider the distance dependence of the intensity of scattered light. These measurements were mainly done in the direction of maximum scattering ($\theta = 90°$) in order to have the maximum signal reach the detector as the detector was moved away from the test tube. Some sample fits to the data obtained with the Newport Power Meter are shown in Fig. 7 for three typical concentrations. These data were taken with the test tube completely covered except for a $d = 3$ mm section facing the detector. We could cover only a distance range from $R = 2$ cm to about 12 cm in this case because the Newport meter could not discern small changes in power with distance at larger distances. The data for all
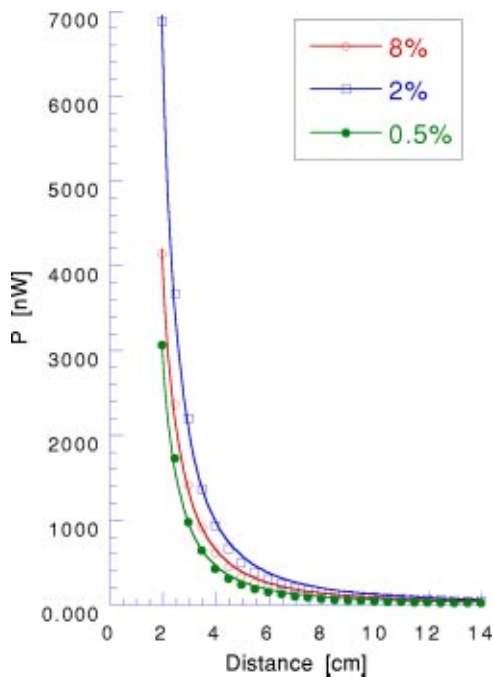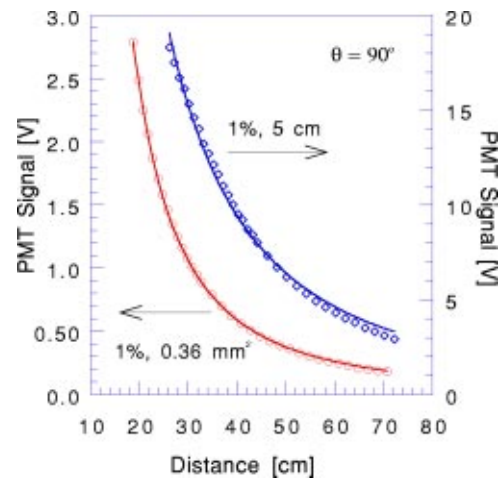

Fig. 7. Plot of power vs distance for three aqueous suspensions of skim milk of different concentrations by volume. The symbols represent measurements and the solid curves represent fits of the function $a/(r+b)^2$ to the data. The power measurements were made with a Newport Power Meter.

three concentrations (and others in between) fit reasonably well to $I(r) = a/(r+b)^2$. The parameter a depends on the beam intensity and the concentration of scatterers and has a different value for each of the data sets. In contrast, the fitting parameter b comes out to be the same, $b = -(0.67 \pm 0.03)$ cm for all three fits. Most of the negative offset (systematic error) in the distance measurements can be accounted for as follows. To prevent stray light from entering the detector, the detector head was covered with black paper containing a 4-mm-diam hole in the center and situated approximately 0.9 cm ahead of the detector diode chip. All distances, however, were measured from the beam center to the detector diode chip. It appears as if the detector chip is effectively located close to the 4-mm-diam aperture itself because the size of the aperture (4 mm) is smaller than the chip size (about 1 cm), and hence all the light that enters through the aperture ultimately arrives at the chip and gets measured. We have consistently observed this apparent shift in detector location in all the cases where we used an aperture in front of the detector, including measurements employing the photomultiplier tube.

The radial data in Fig. 8 were collected using a 1% solution with a photomultiplier tube and much smaller aperture (0.6 mm×0.6 mm instead of 3 mm slit) next to the test tube to realize the condition $d \ll R$ even better. With the photomultiplier tube, we could cover a broader range of distance (20–70 cm) because of its high sensitivity. Over this broader range and with the smaller aperture, our data fit extremely well to $I(r) = a/(r+b)^2$ with $b = -(0.75 \pm 0.06)$ cm. For these data, we did not use an aperture in front of the photomultiplier tube. All distances were measured from the beam center to the axis of the photomultiplier tube. In our side mounted photomultiplier tube, however, the cathode surface was approximately 0.75 cm ahead of the photomultiplier tube axis, thus completely accounting for the fitting parameter $b = 0.75$. We did notice a departure from the $1/r^2$ radial dependence as we increased the size of the exposed scattering region beyond a few millimeters and/or the detector was
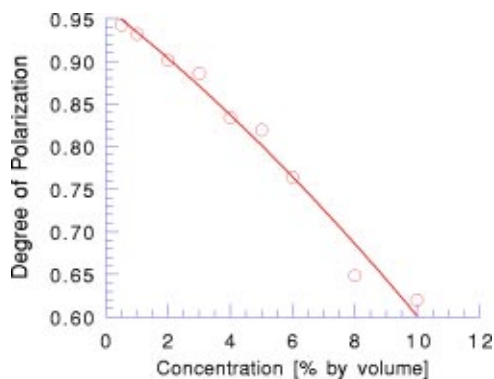
Fig. 9. Plot of degree of polarization vs concentration by volume of milk in aqueous suspension. The solid curve, which is a second-order polynomial fit to the data, is a guide for the eye.

brought too close to the source for $d \ll R$ to hold. An example of this departure, when $d = 5$ cm, is shown in the second curve in Fig. 8.

To summarize, the measured angular and radial distributions of light scattered into the plane perpendicular to the incident polarized laser beam are consistent with the $\sin^2 \theta / r^2$ dependence of electric dipole radiation. We conclude that, for a dilute suspension for which the individual scatterers satisfy the ideal dipole approximation ($s \ll \lambda$), the radiation from the macroscopic system of size $d \ll R$ mimics dipole radiation.

Finally, Fig. 9 shows how the degree of linear polarization of scattered light decreases with increasing concentration of the scatterers. This depolarization of scattered light might be expected for two reasons. First, if there is molecular anisotropy, every scattering event will change the linear polarization of the incident light to an elliptical polarization. Second, because of multiple scattering, which increases with the concentration of scatterers, a given molecule may be driven not only by the **E** field of the primary light, but also by differently oriented **E** fields of scattered light from various directions. Consequently, the electrons in the molecule will vibrate more or less in all directions transversely to the line of sight from the detector. At very small concentrations, the scattered light is polarized horizontally as is the incident light, and the degree of polarization in Fig. 9 is close to unity. As the concentration of scatterers is increased, more and more vertically polarized scattered light is created, and the degree of polarization deteriorates. For similar reasons, wax paper depolarizes the incident polarized light upon transmission. With a further increase in the concentration, milk molecules start to coagulate, forming larger size scatterers that scatter preferentially in the forward direction. In addition, a further increase in concentration results in increased absorption. The end result of all these effects is saturation of laterally scattered light. At high concentrations the beam seems to disappear in a kind of fog.

V. APPLICATIONS

We now briefly describe other versions of the experiment to address different instructional needs. A lecture demonstration version of the experiment has already been discussed in Sec. I. Measurement of the angular distribution can even be performed with an inexpensive photodiode detector[26] and a digital multimeter. In hindsight, we know that only a small portion ($d \ll R$) of the scattering region in the middle should be used and a horizontal polarizer should be mounted in front of the detector to reduce the multiply scattered background. Instead of skim milk, we can also use a suspension of silver nitrate in distilled water. We used a drop of 5% silver nitrate solution in a test tube filled with distilled water and obtained results as good as those presented in Sec. IV. We have not presented the silver nitrate results here in order to avoid repetition, and because silver nitrate is not as readily available as skim milk or milk powder.

There is a variation in which the prism spectrometer is not required. In this version, one rotates the beam polarization instead of the detector to measure the angular distribution.[27] The beam polarization can be rotated by rotating a half waveplate mounted between the laser head and the test tube carrying the suspension. When a polarized beam passes through a half waveplate whose optic axis is oriented at an angle ϕ with respect to the input polarization, the output polarization of the beam is rotated by 2ϕ with respect to the input polarization (see Ref. 12, Chap. 8). Of course, we could directly rotate the laser head itself, but that is relatively inconvenient. In this variation, only an optical rail is required for both angular and radial measurements.

An interesting extension of our experiment would be to carry out angular measurements in a plane perpendicular to the direction of polarization of the laser beam, where we expect an isotropic distribution because $\theta = 90°$ everywhere. To perform this extension, we would need a spherical glass container with flat end caps instead of a test tube. In another possible extension, the test tube carrying the milk suspension could be replaced by a cylindrical vapor cell for studying scattering in gases.

Finally, we comment on how the understanding of dipole radiation helped students to appreciate other related phenomena. A directly related example that students encounter in the lab is the polarization of unpolarized light when scattered at 90° from the beam direction. They check this polarization by replacing the polarized laser with an unpolarized one. If we take the beam direction along the x axis, the electric field of unpolarized light will be oriented (though randomly changing) somewhere in the yz plane and will drive the scatterer charges along its direction. If one is looking at light scattered along the y direction, the only light one will receive is from the component of charge oscillation is in the z direction. This light will be completely polarized along the z axis.

Another example of how dipole radiation is used occurs in the second experiment of our lab course, in which students measure the reflectance of polarized light from a glass surface as a function of incidence angle θ_i. For light polarized parallel to the plane of incidence, they find that the reflectance becomes zero at a certain $\theta_i = \theta_B$, known as Brewster's angle, that is, $R_\parallel(\theta_B) = 0$. It is important to emphasize here that while the transmitted light is mainly the incident light plus some light generated by the oscillations of charges in the glass, the reflected light is entirely created by the glass charges only. If these charges happen to vibrate in the direction of the expected reflection, there would not be any reflection because the charges do not radiate EM energy in the direction of their vibrations. That is exactly what happens at $\theta_i = \theta_B$, because at this angle the **E** field of the transmitted beam that drives the glass charges is in the direction of expected reflection. At θ_B then, the transmittance becomes 100%. This phenomenon is used in Brewster's windows for

polarized lasers. (This phenomenon is very rare, and the only other example occurs at the critical angle where the reflectance becomes unity; it is the basis of step-index fiber optics.) For unpolarized light incident at θ_B, the reflected light will come only from vibrations of charges driven by the **E** field perpendicular ($E_\perp$) to the plane of incidence, and it will be completely polarized perpendicular to the plane of incidence.

Note that $R_\parallel$ and $R_\perp$ are continuous functions of θ_i, with the same value at $\theta_i = 0$ (there is no difference between parallel and perpendicular polarizations at $\theta_i = 0$), and both approaching unity at $\theta_i = 90°$. But because $R_\parallel$ drops to zero at θ_B, $R_\perp$ is much greater than $R_\parallel$, especially around θ_B. For this reason, rainbow light is polarized tangential to the bow—horizontally near the top and vertically near the two lower ends. Sunglasses (polarizers with their transmission axis vertical) eliminate $E_\perp$ which is horizontal when reflection occurs from a horizontal surface such as sand or water on a beach.

Similarly, the intensity and the polarization of radiation from nonrelativistic charges undergoing uniform circular motion can be predicted using dipole radiation concepts. For a charge moving along a circular trajectory, the centripetal acceleration vector of the charge also undergoes a circular motion. If we remember that $\mathbf{E} \propto \mathbf{a}_\perp$, the **E** vector of the radiation field observed at a distant point on the axis of the circle, also will undergo a circular motion about the axis, giving rise to circularly polarized electromagnetic radiation. On the other hand, the radiation field observed at any distant point in the plane of the circle of the rotating charge will be linearly polarized along the diametric projection of the circular trajectory as seen from that point. This linear polarization is observed because the projection of the rotating acceleration vector **a** along a diameter of the circular path is an oscillating vector. For charges moving in a circle at relativistic velocities, as in a synchrotron, the low-speed doughnut pattern $\sin^2 \theta$ angular distribution becomes distorted to a sharply peaked "headlight" in the direction of the velocity.[28] Similarly, the low-speed doughnut pattern of a charge accelerating or decelerating (as in bremsstrahlung) in its direction of motion is tipped forward more and more and increases in magnitude as its speed approaches that of light.[29] At this point, students can be introduced to bursts of polarized electromagnetic waves from astronomical objects such as pulsars and spiraling electrons trapped in radiation belts surrounding the planet Jupiter.

Phase changes on reflection of polarized light from a dielectric surface can similarly be explained. For perpendicular polarization there is an instantaneous phase change of π on reflection because of the negative sign in Eq. (4): $\mathbf{E}_{\text{ref}}(\mathbf{r},t) \propto -\mathbf{a}_\perp(\mathbf{r},t) \propto -\mathbf{E}_{\text{inc}}(\mathbf{r},t)$. For the parallel polarization there is a phase change of π only when θ_i becomes greater than θ_B. This is due to a reversal in the direction of $\mathbf{a}_\perp$ at θ_B.[30] Finally, as discussed earlier, the ω^4 dependence of the dipole radiation explains the blue color of the sky away from the sun and fiery sunrises and sunsets. On the other hand, in the absence of an atmosphere, the lunar sky is pitch-dark.

VI. SUMMARY

We found that the measured angular and radial distributions of light scattered by aqueous suspensions of skim milk into the plane perpendicular to the incident polarized laser

beam are consistent with the $\sin^2 \theta/r^2$ dependence of electric dipole radiation. We are led to conclude that if the individual scatterers of a random collection satisfy the ideal dipole approximation ($s \ll \lambda$), then the radiation from the whole collection of macroscopic size $d \ll R$ mimics dipole radiation. In the limit $d \ll R$, the $\sin^2 \theta/r^2$ dependence is found to hold over a range of concentrations (0.25 to 10%) except for an increase in the background due to multiple scattering.

In addition to presenting variations of this experiment that may serve different instructional needs, we have also suggested some possible extensions. Finally, a number of examples related to this study have been discussed.

[a]Electronic mail: phy_sharma@online.emich.edu

[1]See ⟨http://www.physics.emich.edu/molab/MOLCourse.html⟩ to find a description of this course or ask for a preprint of the Modern Optics Lab Manual by Natthi L. Sharma and Ernest R. Behringer (1999).

[2]D. E. Shaw, M. J. Hones, and F. J. Wunderlich, "Quantitative, molecular light-scattering experiment," Am. J. Phys. **41**, 1229–1232 (1973).

[3]R. M. Drake and J. E. Gordon, "Mie scattering," Am. J. Phys. **53**, 955–962 (1985).

[4]E. K. Hobbie and Lipiin Sung, "Rayleigh-Gans scattering from polydisperse colloidal suspensions," Am. J. Phys. **64**, 1298–1303 (1996).

[5]I. Weiner, M. Rust, and T. D. Donnelly, "Particle size determination: An undergraduate lab in Mie scattering," Am. J. Phys. **69**, 129–136 (2001).

[6]C. L. Adler and J. A. Lock, "A simple demonstration of Mie scattering using an overhead projector," Am. J. Phys. **70**, 91–93 (2002).

[7]Athanasios Aridgides, Ralph N. Pinnock, and Donald F. Collins, "Observation of Rayleigh scattering and airglow," Am. J. Phys. **44**, 244–247 (1976).

[8]A. J. Cox, Alan J. DeWeerd, and Jennifer Linden, "An experiment to measure Mie and Rayleigh total cross sections," Am. J. Phys. **70**, 620–625 (2002).

[9]Craig F. Bohren, "Multiple scattering of light and some of its observable consequences," Am. J. Phys. **55**, 524–533 (1987).

[10]T. V. George, L. Goldstein, L. Slama, and M. Yokoyama, "Molecular Scattering of Ruby-Laser Light," Phys. Rev. **137**, A369–A381 (1965).

[11]Mark P. Silverman, *Waves and Grains* (Princeton University Press, Princeton, NJ, 1998), pp. 288–290.

[12]Eugene Hecht, *Optics* (Addison–Wesley, San Francisco, 2002), Secs. 3.5 and 4.2, especially Fig. 4.8.

[13]John D. Jackson, *Classical Electrodynamics* (Wiley, New York, 1999), Chaps. 9 and 10.

[14]C. F. Bohren and D. R. Huffman, *Absorption and Scattering of Light by Small Particles* (Wiley-Interscience, New York, 1983).

[15]G. Mie, "Beitrage zur optic trüber medien speziell kolloidaler metallösungen," Ann. Phys. (Leipzig) **25**, 377–445 (1908); See also H. C. van de Hulst, *Light Scattering by Small Particles* (Wiley, New York, 1957), pp. 176–178.

[16]David J. Griiffiths, *Introduction to Electrodynamics* (Prentice–Hall, Upper Saddle River, NJ, 1999), Sec. 11.1, or Ref. 13, Sec. 9.2.

[17]Equation (4) is true even for a single accelerated charge q as discussed by R. P. Feynman, R. B. Leighton, and M. Sands, *The Feynman Lectures on Physics* (Addison–Wesley, Reading, MA, 1964), Vol. 1, Sec. 28.2 and Vol. 2, Sec. 21.1. Also see Hans C. Ohanian, "Electromagnetic radiation fields: A simple approach via field lines," Am. J. Phys. **48**, 170–171 (1980). Equation (4) can also be derived by taking the nonrelativistic limit ($v \ll c$) of the radiation fields obtained from the Lienard–Wiechert potentials (see Ref. 16, Sec. 11.2.1). Note that the limit $v \ll c$ for an arbitrarily moving charge is equivalent to the limit $d \ll \lambda$ for the case of oscillatory motion of a dipole source of finite size d. Equation (4) is more general than Eq. (1), and we use it to understand other related phenomena.

[18]A simple qualitative derivation of Eq. (4) is also given by Frank S. Crawford, Jr., *Waves*, Berkeley Physics Course, Vol. 3 (McGraw–Hill, New

York, 1968), Sec. 7.5. This is a wonderful series to read in addition to the Feynman Lectures.

[19]Lord Rayleigh, "On the transmission of light through an atmosphere containing small Particles in suspension, and on the origin of the blue of the sky," Philos. Mag. **47**, 375–384 (1899).

[20]We used a model 818-SL detector along with model 840-C handheld, backlit optical power meter ($1440), Newport Corporation, 1791 Deere Ave., Irvine, CA 92714.

[21]A polarized, single transverse mode (TEM_{00}) laser is required instead of using a randomly polarized laser with an outside polarizer. Although in a polarized laser all the oscillating modes have the same polarization, usually with better than 500:1 polarization purity, in a randomly polarized laser adjacent axial modes are orthogonally polarized and the output is a time-varying mix of modes of different polarizations. Using a polarizer may decrease the power output of a randomly polarized laser to less than half and will not provide the required polarization purity. Also, the laser must be warmed up for at least half an hour to acquire thermal stability or until it gives a stable (within 5%) output before any measurements. Cylindrical laser heads are recommended because they reach thermal equilibrium quickly and are more thermally stable than bare laser tubes. We used a 10-mW polarized He–Ne laser with quoted polarization purity better than 500:1 and maximum mode sweep of 2%. The mode sweep is related to power stability. The model number is MG 05LHP991 (Melles Griot, 1770 Kettering Street, Irvine, CA 92614).

[22]We used a Side-On Hamamatsu R928 photomultiplier tube with model C6270 HV Power Supply Socket Assembly (Hamamatsu, 360 Foothill Road, P.O. Box 6910, Bridgewater, NJ 08807-0910), and a PR 1121 photomultiplier tube Housing (Product for Research, 88 Holten St., Danvers, MA 01923).

[23]Kaleidagraph, Synergy Software, 2457 Perkiomen Ave., Reading, PA 19606 ⟨http://www.synergy.com⟩.

[24]Pieter Walstra and Robert Jenness, *Dairy Chemistry and Physics* (Wiley, New York, 1984), p. 2.

[25]*Dairy Technology: Principles of Milk Properties and Processes*, edited by Pieter Walstra (Marcel Dekker, New York, 1999), Vol. 90, p. 128.

[26]These photodiode-amplifier chips (OPT202) are sold by Burr-Brown for about $8.00 through their distributors, Burr Brown Corp., 6730 S. Tucson Blvd., Tucson, AZ 35706.

[27]This variation was suggested by Dan Spiegel during the 1999 Summer Meeting of the AAPT at Trinity University.

[28]The radiation sweeps around like a locomotive's headlight as the particle goes around the circle. It is nicely illustrated in Figs. 8.8 and 8.9 in M. A. Herald and J. B. Marion, *Classical Electromagnetic Radiation* (Saunders College Publishing, Fort Worth, 1995).

[29]See Ref. 13, Sec. 14.3.

[30]See Ref. 18, pp. 415–418.
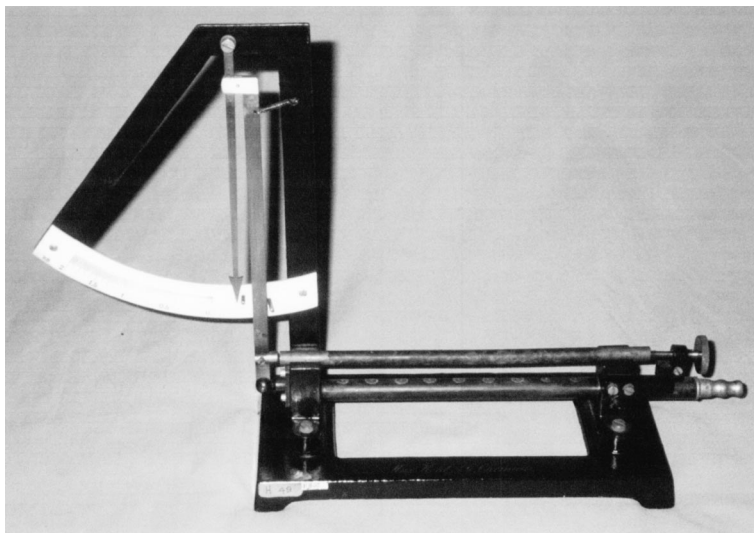
Thermal Expansion Demonstration. This is an example of a *pyrometer*, a device designed to show that metallic bodies expand as their temperature increases. The gas jets underneath the horizontal rod heat the rod fairly uniformly. The rod is held firmly on its right end, and pushes against a multiplying lever on the left end. The instrument can only be used for relative measurements, as there is no way to measure the temperature of the expanding rod. The device was invented by the Dutch physicist Pieter van Musschenbroek (1692–1761). The apparatus is listed in the 1900 Max Kohl catalogue, without the gas burner, at $6.00. It is in the Greenslade Collection. (Photograph and notes by Thomas B. Greenslade, Jr., Kenyon College)